Light-Emitting Coaxial Nanofibers

Haifeng Yang,[†] Carin R. Lightner,[‡] and Liang Dong[†,*]

[†]Laboratory for Nano-Electro-Mechanical Systems and Lab-Chips, Department of Electrical and Computer Engineering and [‡]Department of Chemical and Biological Engineering, Iowa State University, Ames, Iowa 50011, United States

ABSTRACT

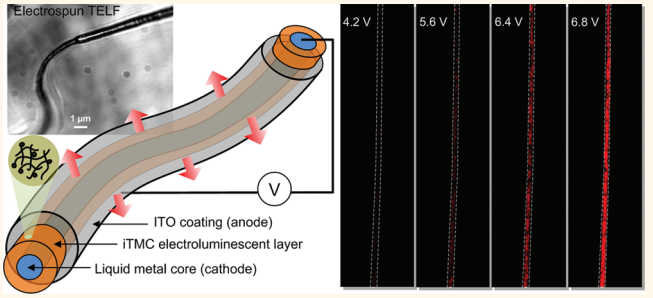

Ionic transition-metal complex (iTMCs)-based electro-luminescent nanofibers (TELFs) are developed by using coelectrospinning. A single TELF consists of a Galistan liquid metal core (cathode), an iTMC-based polymer shell, and an ITO thin film coating (anode). Lights emitted from the TELFs can be detected by a CCD camera at 4.2 V and seen by naked eyes at 5.6 V in nitrogen. The TELFs are structurally self-supporting but do not require a physical substrate (generally relatively bulky and heavy) to support them, rendering one-dimensional light sources more flexible, lightweight, and conformable. This technology can be beneficial to many research and development areas such as optoelectronic textile, bioimaging, chemical and biological sensing, high-resolution microscopy, and flexible panel displays, particularly as iTMCs with emission at different wavelengths are available.

KEYWORDS: electrospinning · nanofibers · light emitting devices · optoelectronic textile · ionic transition-metal complex

Organic light-emitting devices (OLEDs) have been attracting much attention for their remarkable advantages, including full color capability, high efficiency, mechanical flexibility, lightweight, and significant potential for low manufacturing costs.[1−4] In particular, OLEDs having a fiber form factor hold great promise to integrate optical and optoelectronic devices into textile. Recently, fiber-based electroluminescent devices have been built on the surface of an optical fiber with a diameter ranging from a few micrometers to hundreds of micrometers.[5,6] They are fabricated *via* a conventional fabrication route, starting on a substrate followed by sequential deposition and patterning of multiple thin films.[5,6] With a continuing trend toward lightweight and conformable optical and optoelectronic textile technology, smaller, more flexible light sources and many other important optoelectronic devices are being continuously developed, by using different fabrication techniques.[7−15] An excellent example is using preform-based fiber-processing methods to embed multiple layers of conductors, semiconductors, and insulators in a single fiber. The fibers are thermally drawn and share the basic device attributes of their traditional electronic and optoelectronic counterparts such as surface-emitting fiber lasers, photodetectors, and optical resonators.[7−10] Light-emitting nanowires and nanotubes have also been demonstrated *via* template-assisted synthesis,[11] vacuum sublimation,[12] and dip-pen nanolithography.[13] These nanofabrication methods, however, generally suffer from a low throughput.[14] Recently, electrospinning has been employed to develop light-emitting nanofibers with a relatively high throughput.[15] The devices are formed by spinning a polymer nanofiber embedding ruthenium-based ionic transition-metal complex (iTMC) onto an array of microfabricated interdigitated electrodes. This simple method allows the nanofiber to emit discrete lights at interelectrode spacing by applying a voltage to the electrodes.[15] Photoluminescent nanofibers of conjugated polymers, copolymers, and their blends have also been reported, by combining electrospinning and nanoimprint lithography.[14] But they require external optical excitations to emit lights.

Electrospinning is a simple, inexpensive, and effective method for producing fibers with a diameter ranging from several tens of nanometers to a few micrometers.[16−18] This is a popular textile manufacturing process that dates back to the 1930s. Novel applications are being continuously investigated, as morphologies of electrospun fibers (*e.g.*, core−shell,[19−22] side-by-side,[23] and multiple compartment structures[24,25]) can be realized by using modified electrospinning techniques. Particularly, coelectrospinning allows the fabrication of complex fibers

* Address correspondence to ldong@iastate.edu.

Received for review October 21, 2011 and accepted December 23, 2011.

Published online December 23, 2011
10.1021/nn204055t

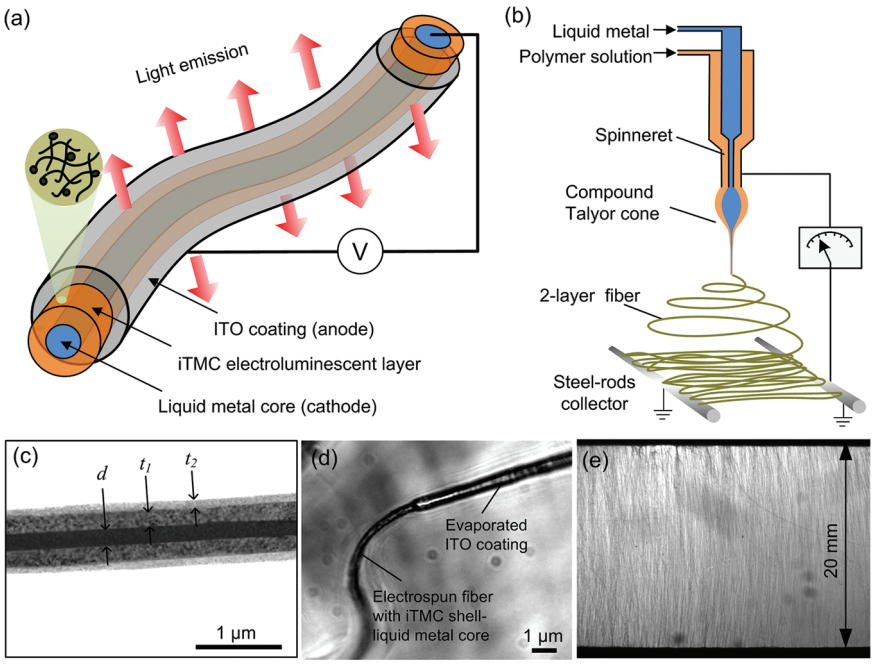

Figure 1. (a) Schematic structure of a TELF. The liquid core contains Gallistane liquid metal as the cathode. The second layer from the core is made of iTMC-based electroluminescent polymer. The device surface is coated with a transparent ITO thin film as the anode by evaporation. The liquid core and polymer shell are formed by coelectrospinning. (b) Schematic setup of coelectrospinning. (c) TEM image of a TELF. (d) Optical image showing the iTMC shell at the end of a TELF. Gallistane liquid metal is encapsulated by the iTMC shell. (e) Optical image showing aligned TELFs across an air gap between two steel rods of a collector (see schematic of fabrication processes in Supporting Information).

with hollow interiors, core–sheath complexes, and tubular multicompartments for use in textile, bioscience, energy harvesting, and storage.[16,26] It is noteworthy that encapsulation of various type of liquids such as drug-containing fluids and liquid crystal in a hollow interior core of electrospun core–shell micro/nanofibers have been reported.[16,27–29]

In this paper, we report on our effort to develop novel iTMCs-based electro-luminescent fibers (TELFs) using coelectrospinning. Figure 1a shows the schematic architecture for the TELF in this study. The device consists of three coaxial layers in a single fiber. The inner hollow core is filled up with highly conductive, continuous phase liquid metal Galinstan (conductivity: $3-4 \times 10^6$ S/m at 20 °C) as the cathode. Galinstan is in a liquid form at room temperature. It consists of 68.5 wt % Ga (work function or WF = ~4.2 eV), 21.5 wt % In (WF = ~4.12 eV), and 10 wt % Sn (WF = ~4.42 eV) with a low melting point at −19 °C. This liquid core is surrounded by a polymer shell of iTMC-based organic electroluminescent material drawn from a mixture of ruthenium(II) tris(bipyridine) $(Ru(bpy)_3]^{2+}(PF_6)^-)_2)$ and poly(ethyl oxide) (PEO). Here coelectrospinning is employed to encapsulate the liquid metal into the Ru–metal complex polymer shell in a single step. The outermost coating is a highly conductive and transparent indium–tin oxide (ITO, WF = ~5.0 eV) thin film as the anode. This coaxial fiber can emit light by applying a voltage between the two electrodes, providing a super flexible one-dimensional submicrometer light source. Generally, iTMCs support all three ionic space charge effects, including charge injection, charge transport, and emissive recombination, thereby exhibiting light emitting properties in a single layer of iTMC between two air-stable electrodes.[30–34] The majority of OLEDs with remarkable performances employed vapor evaporated metals as cathodes. Interestingly, it has been demonstrated by other researchers that using flexible liquid metal as cathodes in OLEDs can increase electrical current and brightness for OLEDs.[35] The use of liquid metal cathodes resulted in sharper metal–organic interfaces than the use of vapor-deposited metal cathodes because metal atoms in liquid cathodes were strongly bound together which provided an energy barrier to minimize diffusion of metal atoms into the polymer.[35] Here in this study, we integrate the Galinstan liquid metal core and the iTMC-based polymer shell into a single fiber. Interestingly, the TELFs are structurally self-supporting, but do not require a physical substrate (generally relatively bulky and heavy) to support them, rendering one-dimensional light sources more flexible, lightweight, and conformable. Additionally, because fabrication processes for making TELFs start in air by coelectrospinning, a wide variety of materials (*e.g.*, glass, metal, clothing, plastic) can be chosen to collect TELFs, having less restriction on surface conditions and material properties of candidate collector materials.

The solution preparation method and electrospinning setup for fabricating the Ru–metal complex shell and liquid metal core are described in Experimental

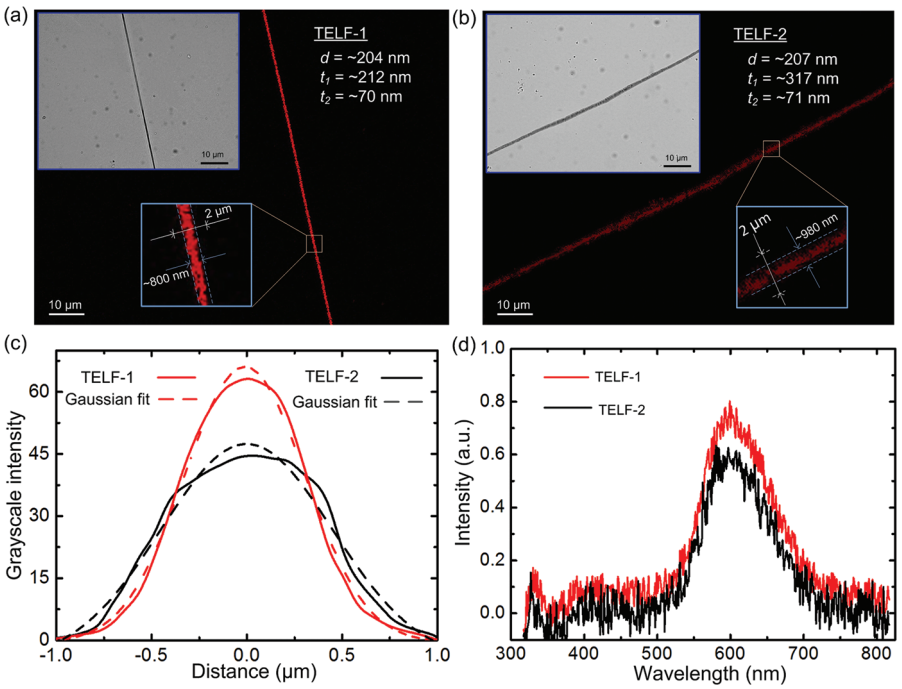

Figure 2. (a,b) Electroluminescence from TELF-1 (a) and TELF-2 (b) captured by a CCD camera. Both devices operate at 6.4 V in N_2. The rectangular inset in each panel shows the optical microscopic image of the corresponding TELF. The squared inset in each panel displays part of light-emitting region of the corresponding TELF. (c) Grayscale intensity profile from a 2 μm-long line crossing transversely TELF-1 (see square inset in panel a), and TELF-2 (see square inset in panel b). (d) Electroluminescence spectra of light emitted from TELF-1 and TELF-2.

Section. Schematic fabrication processes are described in the Supporting Information. Briefly, a spinneret is designed to allow delivery of two solutions independently by syringe pumps. The flow rate for feeding Galistan liquid and $[Ru(bpy)_3]^{2+}(PF_6)^-)_2$/PEO solution into the spinneret is 0.13 and 0.25 mL/h, respectively. The distance between the spinneret and the fiber collector is 8 cm. Here the collector is formed by two parallel steel rods with a 20 mm air gap (Figure 1b and Supporting Information). The spinneret is charged with a voltage of 7.5 kV. A liquid coaxial jet is pulled out of the tip of a compound Taylor cone and stretched and bent by electric field. Solvent evaporation from the thinned jet results in liquid core–polymer shell fibers falling on the collector. The fibers are aligned perpendicular to the axial direction of the two rods because of electrostatic interactions (Figure 1e).[19] Then, the fibers are carried by the rods and transferred into a conventional evaporator for depositing an ITO thin film all over the surface of the fibers. Only the central portion (3 mm long) of the fibers between the two rods is exposed to deposition, while the other portions are masked. Subsequently, 7 mm long fibers are cut by a razor blade and picked up onto a glass slide (Supporting Information). Thus, there is a 2 mm-long region uncovered by ITO on each side of the fibers (Figure 1d). Finally, epoxy (No. 15277, Super Glue, CA) is used to seal the two open ends to avoid leakage of liquid metal. Thus, the TELFs are fabricated. Transmission electron microscopic (TEM) inspection reveals dimensions of the fabricated TELFs as follows (Figure 1c): the diameter of the core d = 204 ± 35 nm; the thickness of the $[Ru(bpy)_3]^{2+}(PF_6)^-)_2$/PEO shell t_1 = 212 ± 43 nm; the thickness of the ITO coating t_2 = 70 ± 12 nm. The total diameter of the TELF is 798 ± 68 nm. By changing the flow rate of Galistan liquid and Ru–metal complex solution to be 0.15 and 0.31 mL/h, respectively, we are able to fabricate thick TELFs with d = 207 ± 27, t_1 = 317 ± 63, and t_2 = 71 ± 15 nm. The source materials and setup for fabricating these thick TELFs are exactly the same as those for fabricating the aforementioned thin ones. We name the thin and thick TELFs "TELF-1" and "TELF-2", respectively.

RESULTS AND DISCUSSION

Experimental testing setup to characterize electroluminescence of the TELFs is described in Experimental Section. Galistan liquid in the core (cathode) is reached by poking the Ru–metal complex shell using a gold-coated atomic force microscope (AFM) tip. To test the device, a voltage is applied between the AFM tip and the ITO coating (anode). Figure 2a,b shows electroluminescence from TELF-1 and TELF-2, respectively. Both are operated at 6.4 V in nitrogen (N_2). Light emission is captured by a CCD camera and analyzed by NIH ImageJ software (National Institutes of Health, Bethesda, Maryland). Emission intensity is represented by grayscale value. Gaussian function is used to fit the curve of grayscale value as a function of distance in transverse direction of each device. The full width at half-maximum (fwhm) amplitude is found to be 855 ± 162 nm

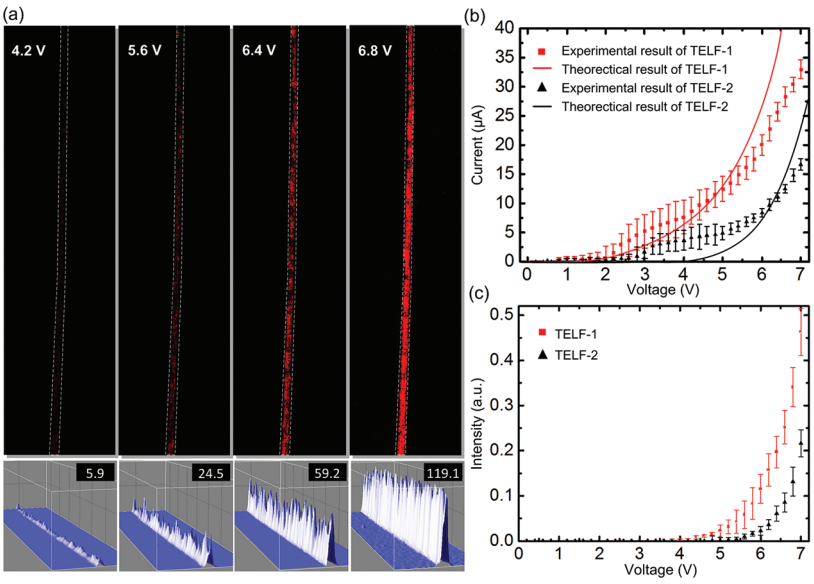

Figure 3. (a) Luminescence responses of TELF-1 to different voltages applied to the device in N_2. The top panels display emissions captured by a CCD camera. The bottom panels show the corresponding emission intensity profiles of the pictures shown in the top panels. The data in the bottom panels represents the mean grayscale emission intensity of the light-emitting region. (b) Experimental and theoretical results for current–voltage characteristics of TELF-1 and TELF-2. (c) Experimental results for current–luminance characteristics of TELF-1 and TELF-2.

for TELF-1, and 984 ± 187 nm for TELF-2 (Figure 2c). The standard deviations of fwhm value are obtained from the measurement results of 14 TELF devices with each device having 20 sampling locations. The result confirms that highly localized emissions are confined within diameter ranges. The grayscale intensity for the light-emitting region of TELF-1 is higher than that of TELF-2 (Figure 2c). Because a higher strength electric field is built in a thinner iTMC layer, more charge carriers are injected into the thin iTMC layer of TELF-1and thus more emissive charge recombinations occur in there. Thus, device dimensions and emission intensity of TELFs are adjustable by tuning coelectrospinning parameters. Luminescence spectra of light emitted from these two devices are measured by a spectrometer (Figure 2d). The characteristic emission wavelength of both devices stays the same at around 598 nm, which is independent of device dimensions.

Figure 3a displays light emission from TELF-1 in response to four different voltages applied in N_2. Notably, light emission is detectable by a CCD camera when TELF-1 operates at as low as 4.2 V. At the operating voltage of 5.6 V, we can see luminescence from the device by naked eyes. The corresponding mean grayscale intensity value for the eye-detectable light-emitting region is 24.5. Clearly, increasing the voltage applied causes an increase in the luminance from the device (top panels in Figure 3a). Actually, the mean grayscale value for the light-emitting region is increased exponentially with the voltage applied, which will be discussed later. Variations in grayscale emission intensity along the axial direction of the TELFs (bottom panels in Figure 3a) is possibly caused by the following factors: nonuniform distribution of $[Ru(bpy)_3]^{2+}(PF_6)^{-})_2$ in PEO matrix, nonuniform transverse dimensions of the devices, and/or a poor coverage of ITO on the device surface.

Current–voltage characteristic of both thin TELF-1 and thick TELF-2 are measured (Figure 3b). Here, the voltage applied to both devices is increased from 0 to 7 V with a step of 0.2 V every 20 s. We find that as the voltage is increased from a lower value to a higher one, the current first fluctuates and then becomes stable in 5–10 s. Given an applied voltage, the thinner the Ru–metal complex layer is, the larger is the current through the device. In both devices, the current is found to first ramp upward while its increasing rate gradually slows down, and then it increases exponentially with increasing voltage applied. A possible explanation to this phenomenon is as follows: initial low voltages cause the redistribution of $PF6^{-}$ ions and establish a first monopolar injection of charge carriers. After the voltage increases further, the current is increased rapidly to trigger a second biopolar injection of charge carriers and thus light emissions.[36] Thereafter, we also measure luminance–voltage characteristic of these two TELFs (Figure 3c). Interestingly, luminescence threshold voltage or turn-on voltage V_{th} of the device is located at the voltage that leads to the aforementioned second carrier injection. V_{th} is 4.2 and 5.4 V for TELF-1 and TELF-2, respectively. Again, emission intensity of TELF-1 is increased faster than that of TELF-2 due to having a thicker iTMC layer. After the devices are lit, their emission intensity follows a trend of exponential increasing with the voltage applied. Theoretical analysis for the current–voltage

characteristics of the TELF-1 and TELF-2 devices is also conducted (see Supporting Information and Figure 3b).[37] The theoretical results are shown to have a similar tendency to the experimental results. The discrepancy between the simulation and experimental results could be explained by intrinsic limitations of the model used and/or misspecifications of the parameters.

Device stability is evaluated by continuously operating TELF-1 in air and N_2, respectively, for a 10 h period each under different voltage conditions (Figure 4). Interestingly, the device presents a lower initial emission intensity and a faster degrading rate when operating in air than it does when operating in N_2. Since there exists a 3 mm-long ITO-uncovered region at each end of the TELF (Supporting Information), partial exposure of the electroluminescent layer to oxygen in air might lead to a significant loss of radiant flux with time.[36] Thus by properly encapsulate the TELF, device stability can be enhanced. Additionally, emission intensity of the device decreases faster at higher voltages than it does at lower ones: 1.1, 2.8, 4.2, and 7.6% degradation in light intensity is found at the applied voltage of 4.2, 5.6, 6.4, and 6.8 V, respectively, in N_2, over the 10 h period. This low level degradation could be attributed to self-heating effect of the device. The higher the operation voltage and current, the higher the power dissipation in the device, and thus the more severe the self-heating effect. However, when the device operates in air, the level of degradation is increased to 1.7, 4.6, 9.2, and 17.2% at the same voltages, respectively, over the same 10-h period. This higher level of degradation is possible owing to both the aforementioned self-heating effect and the oxygen exposure issue. Finally, the external quantum efficiency (EQE) of the $[Ru(bpy)_3]^{2+}(PF_6)^{-})_2$/PEO nanofiber material is calculated on the basis of the amount of light a photodetector captures from the front face of a device. We assume that the emission is Lambertian. The total flux leaving a device F_{ext} at a distance L from the detector is given by[38]

$$F_{ext} = \int_0^{\pi/2} 2\pi L \cos(\theta) \sin(\theta)\, d\theta = \pi L \qquad (1)$$

Since the light collected by the photodiode F is within the emission angles $\theta = 0$ to π, we integrate over these angles and obtain $F/F_{ext} = 0.27$. Then we divide the measured power output by this factor and use the corrected power P in the following equation

$$\eta_{ext} = \frac{P/h\nu}{I/e} \qquad (2)$$

where h is Planck's constant, ν is the center frequency of the emitted radiation, I is the current, and e is the elementary charge. The calculated EQE is approximately 0.277% with a corresponding luminance of 23 cd/m^2. This EQE value is comparable to those reported by other researchers using a blend of Ru complexes and PEO.[15,36,38]

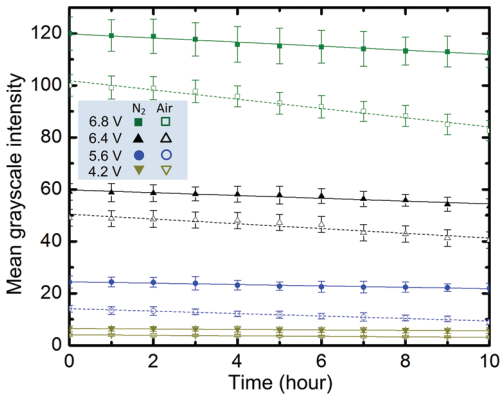

Figure 4. Mean grayscale emission intensity of TELF-1 as a function of time over a 10 h period at four different voltages. The device operates in both air and N_2. Error bars are standard deviations of the mean grayscale intensity obtained from 14 samples.

Much work can be done to elaborate the present TELF technology in the future. For example, to improve the yield of liquid metal core−polymer shell fibers with more uniform diameters and less break-ups, systematic experimental studies are needed to elucidate how each electrospinning process parameter and precursor solution properties (*e.g.*, viscosity, surface tension, solvent-solution miscibility, solution concentration, and solvent vapor pressure) affect morphologies and properties of each layer (*e.g.*, uniformity, break-up).[16] In another example, the innermost and outermost layers of the TELFs serve as the cathode and anode, respectively. Given an iTMC-based light emitting material in the middle layer, the use of thicker electrode layers can give rise to increased electrical conductance of the two electrode layers, shifting the luminescence threshold voltage of the device to lower values. There is a need to investigate the widest possible range of the liquid core (cathode) diameter using coelectrospinning. Also, the present method of accessing the liquid core relies on using an AFM tip, which is fairly inconvenient, but one could make it possible to connect the liquid inside the core to an external liquid reservoir by nanofluidics,[39,40] which may allow addressing the liquid core from outside. Alternatively, highly conductive composite polymers could be electrospun into the fiber to replace the present ITO coating and liquid metal core.[41,42] In addition, the present TELFs are aligned, but are not precisely placed at a specific location demanded. Using some clever existing methods such as near-field electrospinning,[43] we could solve this issue. Finally, although interfacial interactions between many liquid metal cathodes and electroluminescent polymers on a planar surface have been well studied by other researchers,[35] it should be also interesting to investigate their interactions on a cylindrical surface at the submicrometer and even smaller scale.

CONCLUSIONS

We have built one-dimensional electroluminescent device into a single self-supporting fiber at the submicrometer scale *via* coelectrospinning. The cathode of Galistan liquid metal and the electroluminance layer of $[Ru(bpy)_3]^{2+}(PF_6^-)_2$/PEO are uniquely electrospun in a single core−shell fiber. The TELFs are not grown from a substrate, but are fabricated in air and then fall onto a collector. Thus a wide variety of materials can be used for collector TELFs to meet various application needs. Electroluminance from the TELFs can be detected by a CCD camera at a turn-on voltage of 4.2 V and seen by naked eyes at 5.6 V in N_2. Our TELF scheme could shed a light onto development of one-dimensional, micro/nanosized light source for more lightweight, conformable optoelectronic textile. Besides, this technology could be beneficial to many other research and development areas dealing with bioimaging, chemical, and biological sensing, high-resolution microscopy, and flexible panel displays, particularly as iTMCs with emission at different wavelengths are available.[36,44]

EXPERIMENTAL SECTION

Preparation of precursor solutions for TELFs: To prepare Ru−metal complex solution, $[Ru(bpy)_3]^{2+}(PF_6)^-)_2$ is dissolved in dry acetonitrile at a concentration of 58 mM and magnetically stirred at room temperature for 1 h. A 450 nm polycarbonate membrane filter is used to remove unwanted matter. PEO (M_w = 300 000 g/mol) is added to the filtered solution at 1.25 wt %. The mixed solution is magnetically stirred for 30 min to make a homogeneous solution. All Chemicals were purchased from Aldrich and used as received.

Co-electrospinning setup: A needle-in-needle configuration is used to form a spinneret for coelectrospinning. A 21 guage needle is inserted into a 23 guage needle coaxially to a coannular needle assembly. The two needles are trimmed at their exit orifices. The entrance orifice of each needle is sealed by epoxy glue (Super Glue, CA). Then, a microbore tubing is inserted into each needle through a hole punched in the plastic lock portion of needle. The same type of epoxy glue is used to hold the tubing in place. To deliver two source solutions to the spinneret, the solutions are first loaded into 1 mL syringes (BD Biosciences, MD) and then are pumped to the spinneret through the microbore tubings by syringpe pumps (K_d Scientific, KDS 2000). High voltage is supplied by a high voltage source (Gamma High Voltage Research, FL). The collector used here is made of two parallel steel rods (3.175 mm diameter and 10 mm long, SmallParts, FL) spaced by a 20 mm air gap.

Electroluminescence measurement setup: TELFs are placed on the stage of an inverted microscope (IX-81, Olympus, PA) in a dark room. The microscope is located in a glovebox in a dark room. N_2 is flowed to the glovebox from a gas cylinder when needed. A customized electronic probe station with a gold-coated AFM tip (Nanosensors, Switzerland) is attached to the microscope. The AFM tip has a radius of curvature less than 10 nm. The tip is mounted onto a positioning manipulator (MP-225, Sutter Instrument, CA) and connected to a semiconductor characterization analyzer (4200-SCS, Keithley Instruments, OH). To make an electrical contact to the Galistan liquid in the core of the device, the tip is pressed to poke through the polymer shell. Light emitted from the devices is collected through a 50×/0.5NA objective and a 590−650 nm band-pass filter (D620/60 m, Chroma, VT) and acquired using a QICAM color camera (QIC-F-CLR-12-C, QImaging, BC, Canada). Luminescence spectra of TELFs are obtained by a miniature spectrometer (HR4000, Ocean Optics, FL). NIH ImageJ software is used to extract grayscale data from light-emitting regions.

Acknowledgment. We thank the National Science Foundation (ECCS-1102354) for providing final support. We also thank Profs. J. Shinar, R. Shinar, and M. Jeffries-EL, and Mr. B. Britz for helpful discussions.

Supporting Information Available: Schematic description of device fabrication procedures and simulation details for current−voltage characteristics of TELFs. This material is available free of charge *via* the Internet at http://pubs.acs.org.

REFERENCES AND NOTES

1. Shen, Z. L.; Burrows, P. E.; Bulovic, V.; Forrest, S. R.; Thompson, M. E. Three-Color, Tunable, Organic Light-Emitting Devices. *Science* **1997**, *276*, 2009–2011.
2. Muller, C. D.; Falcou, A.; Reckefuss, N.; Rojahn, M.; Wiederhirn, V.; Rudati, P.; Frohne, H.; Nuyken, O.; Becker, H.; Meerholz, K. Multi-colour Organic Light-Emitting Displays by Solution Processing. *Nature* **2003**, *421*, 829–833.
3. D'Andrade, B. W.; Forrest, S. R. White Organic Light-Emitting Devices for Solid-State Lighting. *Adv. Mater.* **2004**, *16*, 1585–1595.
4. Bernius, M. T.; Inbasekaran, M.; O'Brien, J.; Wu, W. S. Progress with Light-Emitting Polymers. *Adv. Mater.* **2000**, *12*, 1737–1750.
5. O'Connor, B.; An, K. H.; Zhao, Y.; Pipe, K. P.; Shtein, M. Fiber Shaped Organic Light Emitting Device. *Adv. Mater.* **2007**, *19*, 3897–3900.
6. Duggal, A.; Levinson, L. M. OLED Fiber Light Source. US Patent 2003, 6538375 B1.
7. Sorin, F.; Shapira, O.; Abouraddy, A. F.; Spencer, M.; Orf, N. D.; Joannopoulos, J. D.; Fink, Y. Exploiting Collective Effects of Multiple Optoelectronic Devices Integrated in a Single Fiber. *Nano Lett.* **2009**, *9*, 2630–2635.
8. Deng, D. S.; Orf, N. D.; Abouraddy, A. F.; Stolyarov, A. M.; Joannopoulos, J. D.; Stone, H. A.; Fink, Y. In-Fiber Semiconductor Filament Arrays. *Nano Lett.* **2008**, *8*, 4265–4269.
9. Abouraddy, A. F.; Bayindir, M.; Benoit, G.; Hart, S. D.; Kuriki, K.; Orf, N.; Shapira, O.; Sorin, F.; Temelkuran, B.; Fink, Y. Towards Multimaterial Multifunctional Fibres that See, Hear, Sense and Communicate. *Nat. Mater.* **2007**, *6*, 336–347.
10. Vohra, V.; Giovanella, U.; Tubino, R.; Murata, H.; Botta, C. Electroluminescence from Conjugated Polymer Electrospun Nanofibers in Solution Processable Organic Light-Emitting Diodes. *ACS Nano* **2011**, *5*, 5572–5578.
11. O'Carroll, D.; Lieberwirth, I.; Redmond, G. Microcavity Effects and Optically Pumped Lasing in Single Conjugated Polymer Nanowires. *Nat. Nanotechnol.* **2007**, *2*, 180–184.
12. Quochi, F.; Cordella, F.; Orru, R.; Communal, J. E.; Verzeroli, P.; Mura, A.; Bongiovanni, G.; Andreev, A.; Sitter, H.; Sariciftci, N. S. Random Laser Action in Self-Organized

Para-sexiphenyl Nanofibers Grown by Hot-Wall Epitaxy. *Appl. Phys. Lett.* **2004**, *88*, 4454–4456.
13. Noy, A.; Miller, A. E.; Klare, J. E.; Weeks, B. L.; Woods, B. W.; DeYoreo, J. J. Fabrication of Luminescent Nanostructures and Polymer Nanowires Using Dip-Pen Nanolithography. *Nano Lett.* **2002**, *2*, 109–112.
14. Di Benedetto, F.; Camposeo, A.; Pagliara, S.; Mele, E.; Persano, L.; Stabile, R.; Cingolani, R.; Pisignano, D. Patterning of Light-Emitting Conjugated Polymer Nanofibres. *Nat. Nanotechnol.* **2008**, *3*, 614–619.
15. Moran-Mirabal, J. M.; Slinker, J. D.; DeFranco, J. A.; Verbridge, S. S.; Ilic, R.; Flores-Torres, S.; Abruna, H.; Malliaras, G. G.; Craighead, H. G. Electrospun Light-Emitting Nanofibers. *Nano Lett.* **2007**, *7*, 458–463.
16. Li, D.; Xia, Y. N. Electrospinning of Nanofibers: Reinventing the Wheel? *Adv. Mater.* **2004**, *16*, 1151–1170.
17. Ko, F.; Gogotsi, Y.; Ali, A.; Naguib, N.; Ye, H. H.; Yang, G. L.; Li, C.; Willis, P. Electrospinning of Continuons Carbon Nanotube-Filled Nanofiber Yarns. *Adv. Mater.* **2003**, *15*, 1161–1165.
18. Subbiah, T.; Bhat, G. S.; Tock, R. W.; Pararneswaran, S.; Ramkumar, S. S. Electrospinning of Nanofibers. *J. Appl. Polym. Sci.* **2005**, *96*, 557–569.
19. Li, D.; Xia, Y. N. Direct Fabrication of Composite and Ceramic Hollow Nanofibers by Electrospinning. *Nano Lett.* **2004**, *4*, 933–938.
20. Yu, J. H.; Fridrikh, S. V.; Rutledge, G. C. Production of Submicrometer Diameter Fibers by Two-Fluid Electrospinning. *Adv. Mater.* **2004**, *16*, 1562–1566.
21. Sun, Z. C.; Zussman, E.; Yarin, A. L.; Wendorff, J. H.; Greiner, A. Compound Core−Shell Polymer Nanofibers by Co-electrospinning. *Adv. Mater.* **2003**, *15*, 1929–1932.
22. Loscertales, I. G.; Barrero, A.; Marquez, M.; Spretz, R.; Velarde-Ortiz, R.; Larsen, G. Electrically Forced Coaxial Nanojets for One-Step Hollow Nanofiber Design. *J. Am. Chem. Soc.* **2004**, *126*, 5376–5377.
23. Liu, Z. Y.; Sun, D. D.; Guo, P.; Leckie, J. O. An Efficient Bicomponent TiO_2/SnO_2 Nanofiber Photocatalyst Fabricated by Electrospinning with a Side-by-Side Dual Spinneret Method. *Nano Lett.* **2007**, *7*, 1081–1085.
24. Zhao, Y.; Jiang, L. Hollow Micro/Nanomaterials with Multilevel Interior Structures. *Adv. Mater.* **2009**, *25*, 3621–3638.
25. Zhao, Y.; Cao, X. Y.; Jiang, L. Bio-mimic Multichannel Microtubes by a Facile Method. *J. Am. Chem. Soc.* **2007**, *129*, 764–765.
26. Dror, Y.; Salalha, W.; Avrahami, R.; Zussman, E.; Yarin, A. L.; Dersch, R.; Greiner, A.; Wendorff, J. H. One-step Production of Polymeric Microtubes by Co-electrospinning. *Small* **2007**, *3*, 1064–1073.
27. Yang, H.; Dong, L. Smart Drug Delivery Using Electrospun Hollow Nanofibers. *IEEE 23rd Int. Conf. Micro Electro Mech. Syst. Tech. Dig.* **2010**, 308–311.
28. Yarin, A. L.; Zussman, E.; Wendorff, J. H.; Greiner, A. Material Encapsulation and Transport in Core−Shell Micro/Nanofibers, Polymer and Carbon Nanotubes and Micro/nanochannels. *J. Mater. Chem.* **2007**, *17*, 2585–2599.
29. Lagerwall, J. P. F; McCann, J. T.; Formo, E.; Scalia, G.; Xia, Y. N. Coaxial Electrospinning of Microfibres with Liquid Crystal in the Core. *Chem. Commun.* **2008**, 5420–5422.
30. Bernards, D. A.; Flores-Torres, S.; Abruna, H. D.; Malliaras, G. G. Observation of Electroluminescence and Photovoltaic Response in Ionic Junctions. *Science* **2006**, *313*, 1416–1419.
31. Bolink, H. J.; Cappelli, L.; Coronado, E.; Gratzel, M.; Nazeeruddin, M. K. Efficient and Stable Solid-State Light-Emitting Electrochemical Cell Using Tris(4,7-diphenyl-1,10-phenanthroline)ruthenium(II) Hexafluorophosphate. *J. Am. Chem. Soc.* **2006**, *128*, 46–47.
32. Tamayo, A. B.; Garon, S.; Sajoto, T.; Djurovich, P. I.; Tsyba, I. M.; Bau, R.; Thompson, M. E. Cationic Bis-Cyclometalated Iridium(III) Diimine Complexes and Their Use in Efficient Blue, Green, and Red Electroluminescent Devices. *Inorg. Chem.* **2005**, *44*, 8723–8732.
33. Dick, D. J.; Heeger, A. J.; Yang, Y.; Pei, Q. B. Imaging the Structure of the P−N Junction in Polymer Light-Emitting Electrochemical Cells. *Adv. Mater.* **1996**, *8*, 985–987.
34. Gorodetsky, A. A.; Parker, S.; Slinker, J. D.; Bernards, D. A.; Wong, M. H.; Malliaras, G. G.; Flores-Torres, S.; Abruna, H. D. Contact Issues in Electroluminescent Devices from Ruthenium Complexes. *Appl. Phys. Lett.* **2004**, *84*, 807–809.
35. Andersson, G. G.; Gommans, H. H. P.; van der Gon, A. W. D; Brongersma, H. H. Liquid Metals as Electrodes in Polymer Light Emitting Diodes. *J. Appl. Phys.* **2003**, *93*, 3300–3307.
36. Slinker, J. D.; Rivnay, J.; Moskowitz, J. S.; Parker, J. B.; Bernhard, S.; Abruna, H. D.; Malliaras, G. G. Electroluminescent Devices from Ionic Transition Metal Complexes. *J. Mater. Chem.* **2007**, *17*, 2976–2988.
37. Buda, M.; Kalyuzhny, G.; Bard, A. J. Thin-Film Solid-State Electroluminescent Devices Based on Tris(2,2′-Bipyridine) ruthenium(II) Complexes. *J. Am. Chem. Soc.* **2002**, *124*, 6090–6098.
38. Lyons, C. H.; Abbas, E. D.; Lee, J. K.; Rubner, M. F. Solid-State Light-Emitting Devices Based on the Trischelated Ruthenium(II) Complex. 1. Thin Film Blends with Poly-(ethylene oxide). *J. Am. Chem. Soc.* **1998**, *120*, 12100–12107.
39. Eijkel, J. C. T.; van den Berg, A. Nanofluidics: What Is It and What Can We Expect From It? *Microfluid Nanofluid* **2005**, *1*, 249–267.
40. So, J. H.; Dickey, M. D. Inherently Aligned Microfluidic Electrodes Composed of Liquid Metal. *Lab Chip* **2011**, *11*, 905–911.
41. Gangopadhyay, R.; De, A. Conducting Polymer Nanocomposites: A Brief Overview. *Chem. Mater.* **2000**, *12*, 608–622.
42. Laforgue, A.; Robitaille, L. Production of Conductive PEDOT Nanofibers by the Combination of Electrospinning and Vapor-Phase Polymerization. *Macromolecules* **2010**, *43*, 4194–4200.
43. Sun, D.; Chang, C.; Li, S.; Lin, L. Near-Field Electrospinning. *Nano Lett.* **2006**, *6*, 839–842.
44. Friend, R. H.; Gymer, R. W.; Holmes, A. B.; Burroughes, J. H.; Marks, R. N.; Taliani, C.; Bradley, D. D. C.; Dos Santos, D. A.; Bredas, J. L.; Logdlund, M.; *et al.* Electroluminescence in Conjugated Polymers. *Nature* **1999**, *397*, 121–128.